

Zhao Yiran¹², Mi Baigang¹², Zhan Hao¹², Xu Heyong¹²

¹School of Aeronautics, Northwestern Polytechnical University, Xi'an 710072, China ² National Key Laboratory of Aircraft Configuration Design, Xi'an 710072, China

Abstract

The flight state perception model is a critical component of autonomous flight and UAV technology. By precisely gauging the flight state, the autonomous flight system is enpowered to make informed decisions and exercise autonomous control, ultimately elevating the autonomy and intelligence of UAVs. The co-flow jet (CFJ) technology, an active flow control method proposed in the early 21st century, has shown significant lift enhancement effects with minimal power consumption, showing considerable engineering application value. In this study, flight state perception models for CFJ airfoils have been built using deep neural networks. These models can accurately predict typical flight state parameters of a CFJ airfoil, relying solely on a few pressure values measured on the airfoil's surface. To fortify the robustness of the models, a fault diagnosis method based on the random forest classification algorithm is developed. This method offers impeccable accuracy in identifying faulty pressure points. Furthermore, a fault diagnosis and tolerance system for the flight state perception model of the CFJ airfoil is constructed. This system can not only enhance the model's performance and accuracy in scenarios where pressure measurement points malfunction, but also ensures precise predictions of flight conditions, ultimately promoting flight safety in practical applications..

Keywords: flight state perception, fault diagnosis, machine learning, co-flow jet

1. Introduction

Large fixed-wing aircrafts are often equipped with air data systems, such as airspeed head, AoA sensor, atmospheric total temperature detector and so on. But for UAVs, there are often strict requirements for size, weight, power consumption and cost. Therefore, there is a great need for a flight state parameter estimation system, which requires only a small number of sensors to obtain reasonably accurate estimates of flight state parameters.

Flush Air Data Sensing (FADS) system, a method which can estimate flight state parameters based on distributed pressure or velocity sensors, boasts characteristics such as a wide range of airspeed estimates, high precision, and minimal time delay. This method gives up sensing equipment such as the Pitot tube that impacts the aerodynamic shape, directly solving the problem of aircraft dependence on external data for estimating flight parameters. It also reduces radar reflection area, making it a significant research focus for future aircraft flight parameter estimation.

The rudiment of FADS appeared in the 1960s^[1]. Researchers added a static pressure port to the nulling sphere, and the static port was calibrated to measure Mach number and pressure altitude. This research blazed a trail to FADS. However, the research result did not show much positive effect because of its complicated mechanical structure and ball-nose lip interference. By the 1980s, Brown et al.^[2] improved the research by utilizing the sensing probe formed by an array of five pressure holes. This method performed better than single pressure port. Since the researchers merely applied this method to Sabreliner aircraft, Larson et al. ^[3] employed FADS to F-14 airplane at transonic speed and evaluated the ability to obtain air data of FADS. The results indicated that after careful calibration, the FADS with pressure sensor array can provide accurate flight state information such as angle of

attack and angle of sideslip.

In the 1990s, the research focus of FADS turned into error analysis and high precision method exploration. Additionally, the application range of FADS broadened to supersonic speed flight. Initially, Larson et al.^[4] further assessed the feasibility of FADS on the basis of paper [3] through wind tunnel tests. The researchers displayed the estimated value and true value of stagnation pressure, static pressure, angle of attack, angle of sideslip and Mach number in the tabular form. What's more, the cause of the error and its way of coping were discussed. Then, Whitmore er al.^[5] equipped F-18 airplane with FADS consisting of 25 pressure ports, and these ports were arranged in concentric circles at the nose. This research indicated that nine-port data can accurately estimate the air data. Besides, this paper firstly developed fault detection and fault tolerance techniques. Later, authors ^[6] conducted uncertainty and feasibility studies of FADS for hypersonic flight, highlighting its potential accuracy if surface heating is avoided.

In the late 1990s, Rohloff and Catton^[7] developed a neural-network-based FADS system, making the first use of techniques other than semiempirical FADS techniques, and it was proved that a trained network could adequately represent the mapping relationship between several pressure measurements and flight parameters. Rediniotis et al.^[8] then devised a neural-network-based calibration algorithm for FADS, and the networks have features of flexibility in network architecture design and self-optimization capabilities. Over the transition from the 20th century to the present, researchers delved into diverse FADS models, and fault diagnosis methods were developed and further perfected as well. They successfully deployed the system on a range of aircraft, including mini air vehicles^[9], transatmospheric vehicles^[10], and others. Besides, with the advancement of machine learning, there was a tendency that more and more researchers apply machine learning algorithm to build FADS^{[9][11]}, resulting in confirmed satisfactory prediction accuracy.

Co-flow Jet (CFJ), a newly active flow control method proposed in the early 21^{st[12]} century, has demonstrated effectiveness in lift enhancement and drag reduction. After years of development, CFJ is mainly studied as an open-loop control method, lacking adjustability when flight conditions change. To further enhance the application value of CFJ, the exploration of closed-loop control methods is warranted. Accurate flight parameters measurements of the CFJ airfoil, facilitating inputs for closed-loop control systems, is pivotal for preparatory measures. As evidenced in the literature, machine learning algorithms emerge as favorable options for FADS development due to their ease of implementation and ability to provide intricate mappings between vector spaces^[13]. Consequently, this study principally concentrates on constructing a flight state perception model (which is also known as FADS) for the CFJ0012 airfoil using deep neural networks, coupled with fault diagnosis and tolerance methods to enhance the model's robustness.

2. Construction of Flight State Perception Models

In this paper, all numerical simulations are carried out using Ansys Fluent software. The Reynolds-averaged Navier-Stokes (RANS) equations, along with the Spalart-Allmaras (SA) turbulence model, are employed to validate the numerical method for the CFJ0012 airfoil. The numerical method and calculation grid are same to what has been used in Ref [14], and they have been proved to be resultful.

2.1 The selection of pressure measuring points

The purpose of building flight state perception models is to obtain flight state parameters through pressure value of pressure probes on the surface of the airfoil. It is necessary to take both economy and feasibility into account in engineering practice, and it is unrealistic to set pressure probes all around the airfoil, therefore, the number of pressure probes should be minimized. At the same time, it is also necessary to ensure that the selected pressure measurement points are sensitive to the change of flight state parameters.

When selecting pressure probes, two standards should be followed: 1. steep pressure gradients; 2. high pressure variance. The first criterion states that the flow state at the point changes dramatically with the change of flight state; the second criterion indicates that when the flight state changes, the pressure value of this point is highly dispersed. Through the above two standards, the pressure

probes which are relatively sensitive to the change of flight state can be selected.

This paper sets Mach number Ma (ranging from 0.2 to 0.5 with an interval of 0.1), jet momentum coefficient C_{μ} (ranging from 0.01 to 0.2 with an interval of 0.01), height H (ranging from 0km to 8km with an interval of 2km) and angle of attack AoA (ranging from 0° to 20° with an interval of 1°) as research variables. Then, 8400 (5×4×5×21) groups of flight states are sampled uniformly and they are used as calculation condition of CFD. Whereafter, the pressure gradient of each grid point around the airfoil is compared in order to select the position with large pressure gradient, roughly estimate the area where the sensitive pressure probes situate. Finally, by comparing the variance values of the pressure values of each grid point, points with large pressure variance are selected, and the location of the pressure measuring points which are more sensitive to the change of flight state is further reduced and determined.

(1) Surface pressure gradient analysis of airfoil

To identify regions that meet the first criterion, the C_p distribution on the CFJ0012 airfoil is calculated. Figure 1 shows the C_p distribution on the CFJ0012 airfoil under various flight conditions. Each figure within the set illustrates the C_p curve with the variation of a single factor. It can be seen that Figure 1 (a)-(d) show the same law, that is, areas where near the leading edge and the trailing edge, as well as the injection and suction slots, show steep pressure gradient, therefore, the pressure probes should lie within the locations mentioned above.

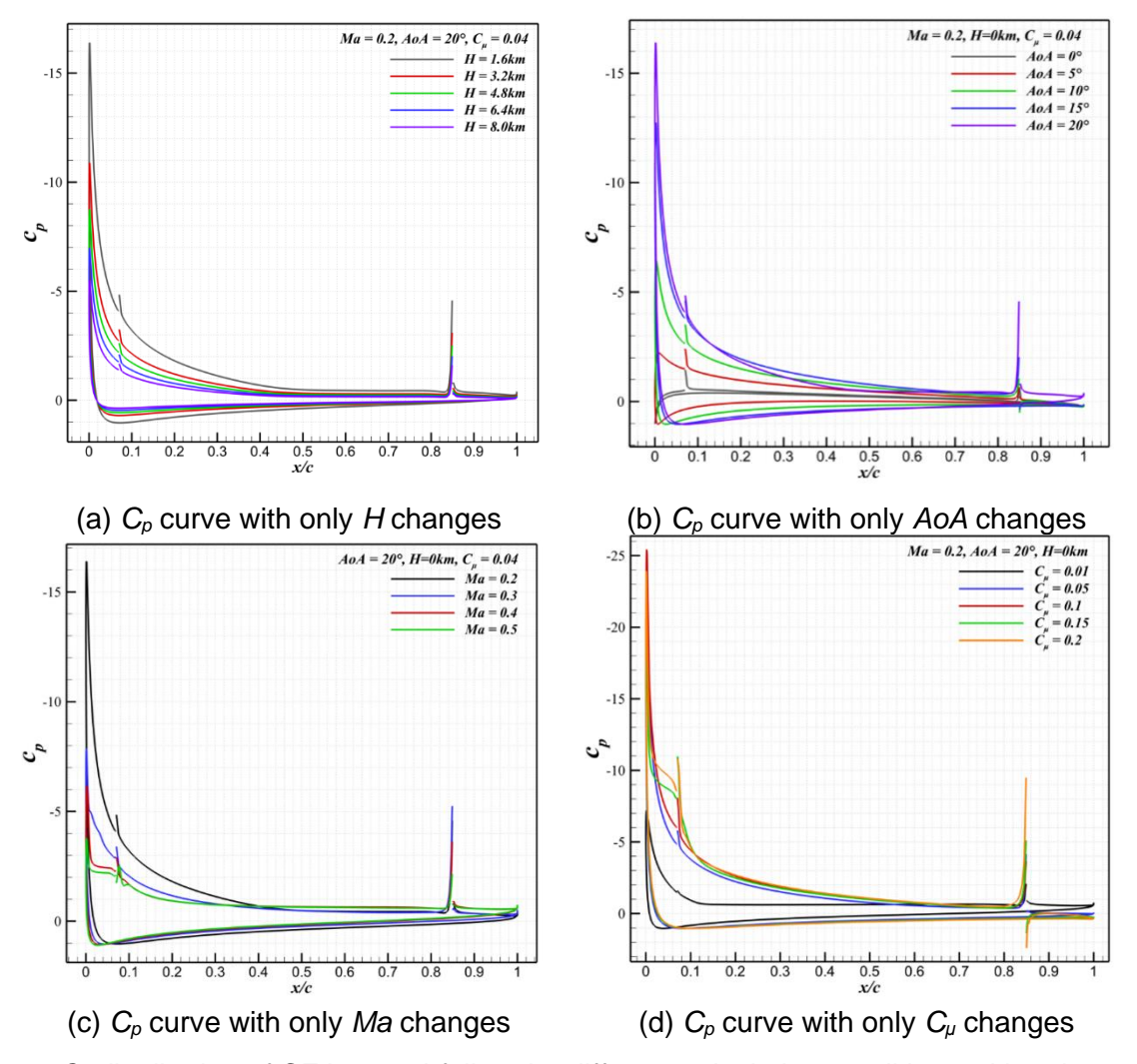


Figure 1 - C_p distribution of CFJ0012 airfoil under different calculating conditions with only one factor changes.

(2) Analysis of variance of airfoil surface pressure

The pressure probes which are sensitive to the change of flight parameters should also be the points where the pressure data is dispersed with the change of flight states. The regions of probes can be further narrowed down by obtaining the pressure variance. The result of pressure variance is shown in Figure 2. From the figure, the pressure probes such as P32, P40, P116, P165 and P300 are selected.

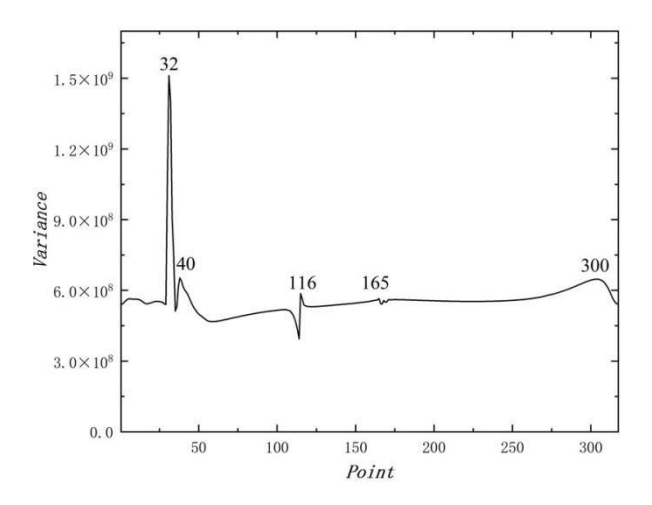


Figure 2 – Calculation result of pressure variance of mesh points on airfoil surface.

Finally, considering both the pressure gradient and pressure variance, 10 pressure probes which are sensitive to the change of flight states are selected, and the locations of them are displayed in Figure 3. P1, P7, P285 and P300 lie near the leading edge, and they can capture dramatic flow changes near the leading edge; P32 and P116 situate at the injection slot and suction slot respectively, both of their locations experience large pressure gradient and high pressure variance; P40, P57 and P104 can feel the change of jet intensity; P163 is at the trailing edge of the airfoil, and trailing edge is also the area which experiences large pressure gradient and high pressure variance.

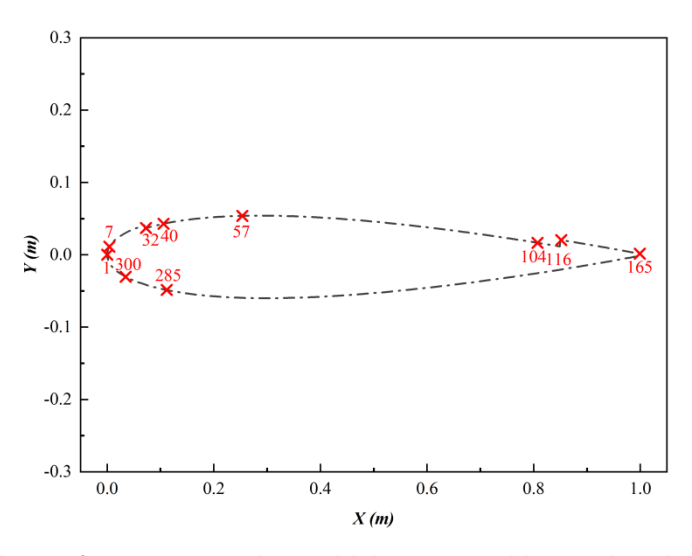


Figure 3 – Locations of pressure probes which are sensitive to the change of flight states.

2.2 Data sets Formation of Flight State Perception Models based on Kriging Model

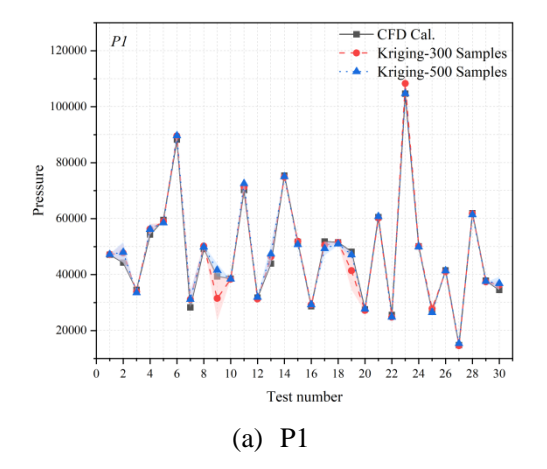
Deep learning is a research orientation in the field of Machine Learning. Deep learning uses multilayered neural networks trained with large data sets to solve complex information processing tasks and has emerged as the most successful paradigm in the field of machine learning. The Deep

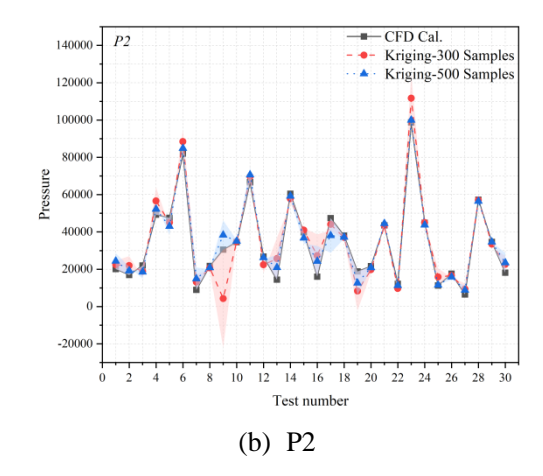
Neural Network (DNN) is a kind of frame of deep learning, and it has at least two hidden layers. The DNN can build models for complex nonlinear systems. In comparison to shallow neural networks, the additional layers in deep neural networks offer a heightened level of abstraction, enhancing the model's capacity for stronger modeling capabilities. As the modeling of flight state perception is a complex and nonlinear task, therefore, this paper intends to apply DNNs to the model construction process of flight state perception models.

To build models based on DNNs, large data sets are needed. To improve the efficiency of generating data sets, this paper uses Kriging algorithm provided by DACE toolbox of Matlab software to build ten Kriging models ($\{Ma, C_{\mu}, H, AoA\} \rightarrow \{P_i\}_{i=1,2,\dots,10}$), then the data set used for DNN modeling will be generated through the Kriging models mentioned above. The detailed modeling process is listed as follows.

- (1) Use Latin Hypercube Sampling (LHS) to acquire a certain amount of flight state groups $\{Ma, C_{\mu}, H, AoA\}$. Then those flight state groups are used as calculation states of CFD numerical simulations. After numerical simulations, pressure values of ten selected pressure points on the surface of CFJ0012 airfoil is obtained.
- (2) Use Kriging algorithm to build ten Kriging surrogate models $\{Ma, C_{\mu}, H, AoA\} \rightarrow \{P_i\}_{i=1,2,\dots,10}$. The inputs of Kriging models are flight state groups sampled before, and the responses are pressure values of ten pressure points.
- (3) Validate the accuracy of ten Kriging surrogate models. After ten Kriging surrogate models are built, use LHS to get several new flight state groups and consider them as the test sample. Then another round of CFD numerical simulations is needed to get pressure values of the test sample. Afterwards, take newly sampled flight states as inputs of Kriging models built in second step, then the corresponding pressure values will be generated as outputs of Kriging models. Compare the pressure values generated by Kriging models with CFD results to validate the accuracy of Kriging models. If the accuracy of Kriging models is satisfied, then data sets of DNN models can be generated by those Kriging models. However, if the model accuracy is low, then some measures should be adopted (such as increasing sample points, changing other regression functions or correlation models) to promote the model accuracy.

This paper constructs two types of Kriging models using 300 and 500 sample points, respectively. Both models employ a second-order polynomial as the basis function for the regression function, with a Gaussian correlation model. The test results of the Kriging models are shown in Figure 4(a)-(j), showing error bands between the predicted value of each model and CFD values. It can be intuitively seen that for the majority of models, the predicted pressure values by the Kriging models closely match the CFD values, and the model accuracy improves with an increase in sample points.





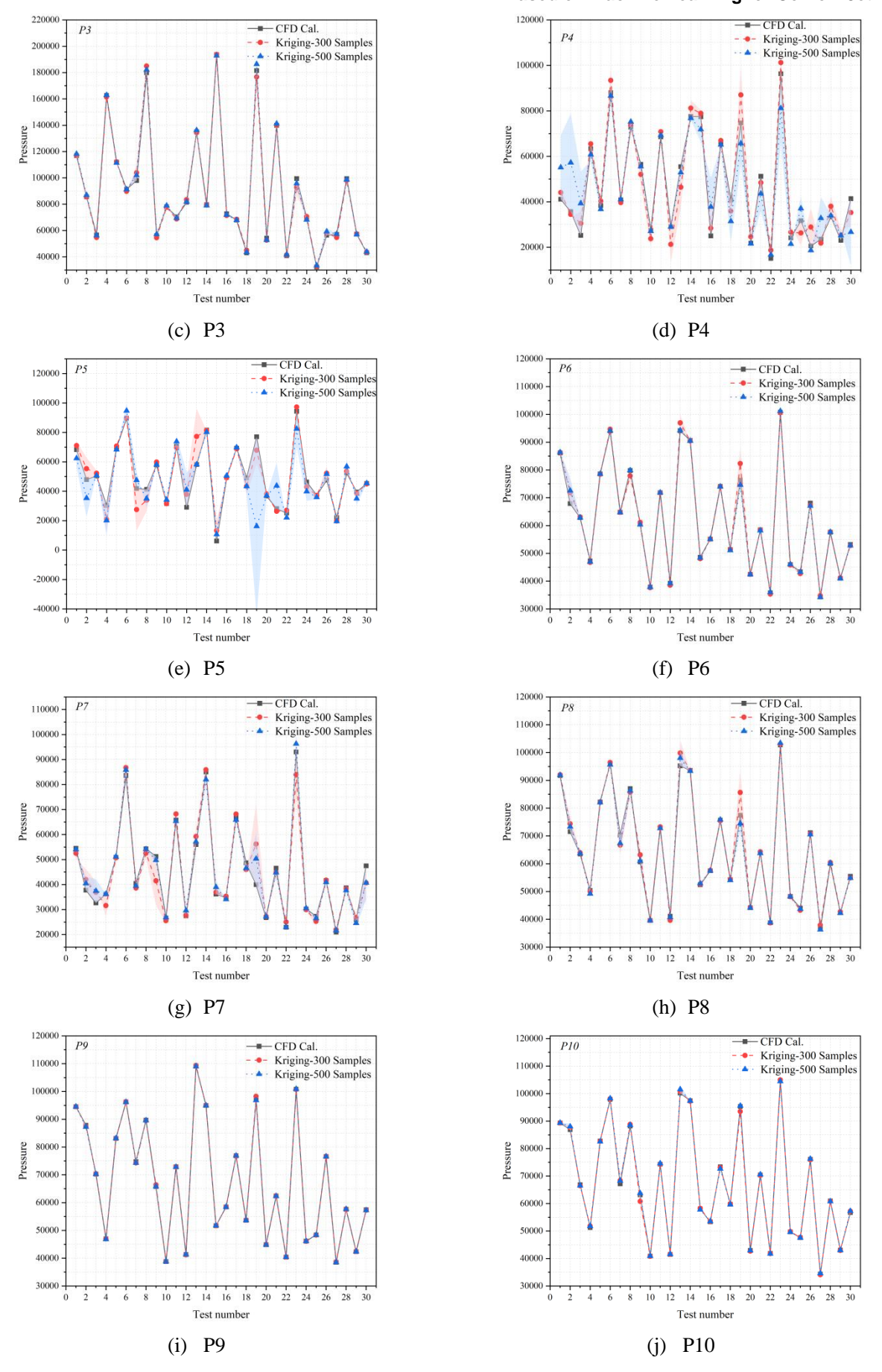


Figure 4 - Comparison between the predicted value of Kriging model constructed with 300 sample points and 500 sample points and the calculated value of CFD.

Since the previously constructed Kriging model will be utilized to generate training samples for the flight state perception model, and the accuracy of these samples directly influences the prediction accuracy of the DNN model, it is imperative to exclude pressure measurement points P2, P4, P5 and P7 with poor prediction accuracy. The remaining pressure measuring points, P1, P3, P6, P8, P9 and P10, characterized by high accuracy, will be employed in subsequent deep neural network training. The coordinates of the six pressure measurement points used to construct the flight state perception model are shown in Table 1.

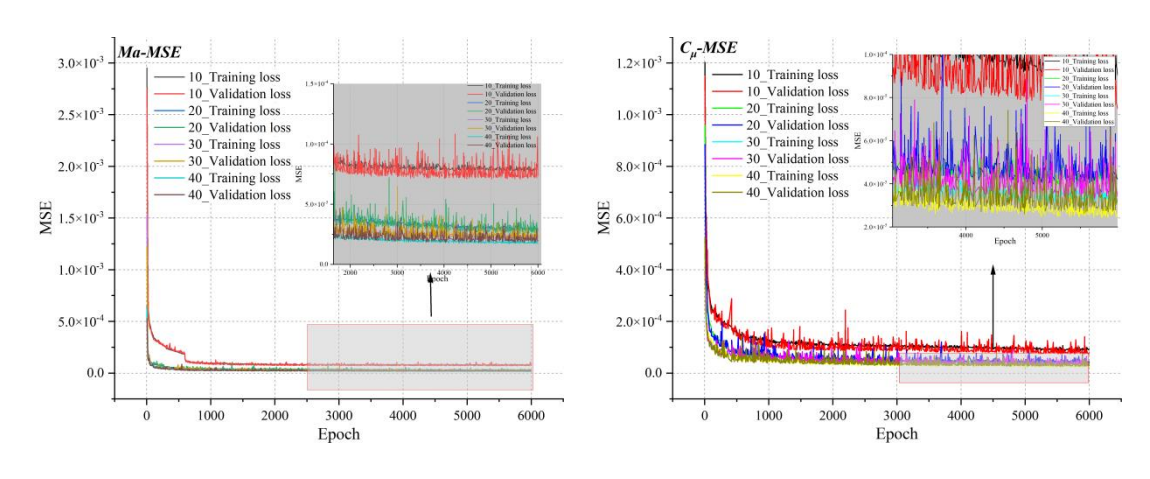
Table 1- The coordinates of six pressure measuring points used to construct the flight state perception models.

Number of pressure point	x coordinate (m)	y coordinate (m)
1	0	0
2	0.07293	0.03690
3	0.80718	0.01661
4	0.99892	0.00140
5	0.11169	-0.04869
6	0.03470	-0.03031

2.3 The Realization of Deep Learning Algorithm used for Building Flight State Perception Models

In this section, the Kriging models built in Section 2.2.1 are employed to generate 20,000 samples for subsequent training of flight state perception models. These samples are categorized into training, testing and validation sets, with an 8:1:1 ratio. To build DNN models, Tensorflow is used. Each DNN contains two hidden layers. The loss function used is Mean Squared Error (MSE), with the Adam optimizer used as the parameter optimizer and Relu as the activation function. In order to ensure the accuracy of DNNs, a "multi-input, single-output" strategy is adopted for constructing flight state perception models, that is, the input is the pressure value of six pressure measurement points, and the output is one of the flight state parameters.

Different numbers of neurons are utilized to train each flight state perception neural network. The MSE curves of the corresponding training validation sets of neural networks are shown in Figure 5. It is observed from the figure that, for the Mach number, jet momentum coefficient and angle of attack neural networks, their MSE curves decrease significantly as the number of neurons increases from 10 to 20. When the number of neurons increases from 20 to 40, the MSE value does not change greatly. Generally, these three groups of neural networks exhibit a trend where more neurons result in smaller MSE values. However, for the height neural networks, the training situations differ from the other groups: when the number of neurons increases from 10 to 20, the MSE increases instead of decreasing. When the number of training epochs is less than 4000, a larger number of neurons correlates with smaller MSE values. Conversely, when the number of training epochs exceeds 4000, the MSE of the model with 30 neurons exhibits a noticeable downward trend, eventually surpassing the performance of the model with 40 neurons.



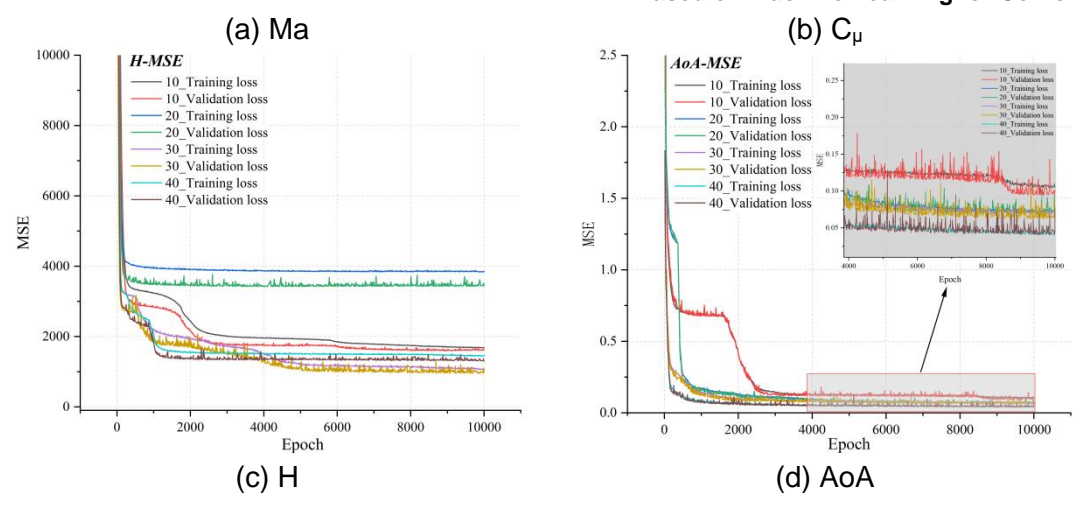


Figure 5 - The MSE curve of training set and validation set of flight state perception neural networks.

To assess model accuracy and select the most precise ones, Figure 6 (a)-(d) displays relative error box diagrams for each model with varying numbers of neurons. The figures reveal that for the Mach number and jet momentum coefficient models, accuracy increases with more neurons. However, the precision of the height and AoA models appears unrelated to neuron count. Notably, the height model exhibits significant instability, with its average relative error surpassing upper and lower limits, attributed to the wide data sample range (0 - 8 km) for height. When height values are small, even though absolute errors may not be significant, smaller denominators in relative error calculations inflate relative error values, resulting in outliers that elevate the average value.

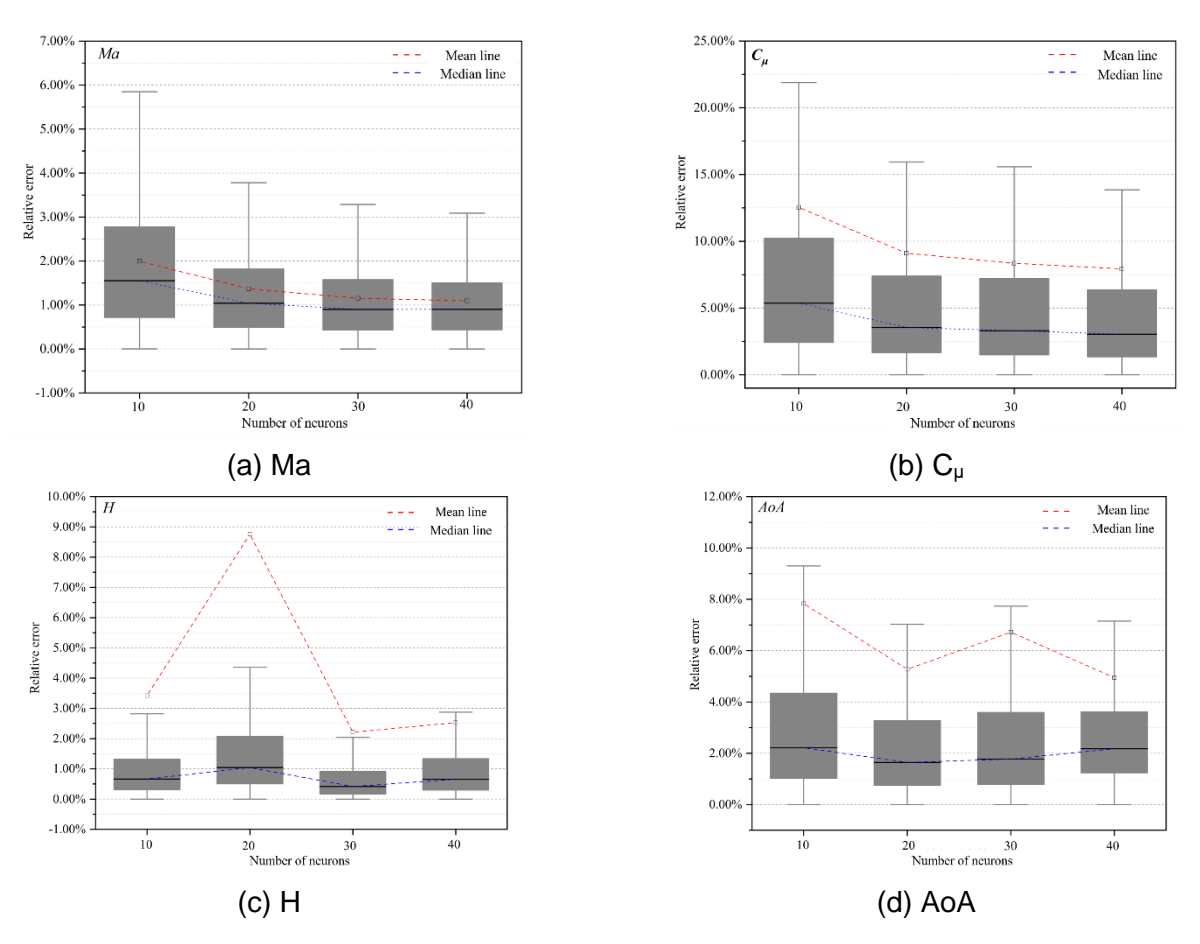


Figure 6 – The relative error box diagram of each flight state perception model with different number of neurons.

To deal with the problem of large relative error, the height is converted to static pressure through Eq. (1).

$$P_{s} = 1013.25 \times e^{-\frac{h}{8431}} h P a \tag{1}$$

The relative error box diagram of static pressure converted from height is shown in Figure 7. It can be seen that the relative error at this time is significantly reduced, the average value is within the box, and the relative error of the outliers is within an appropriate range.

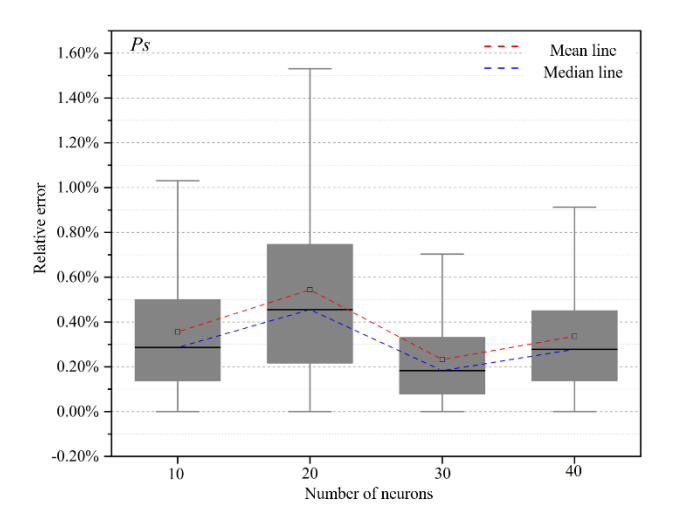
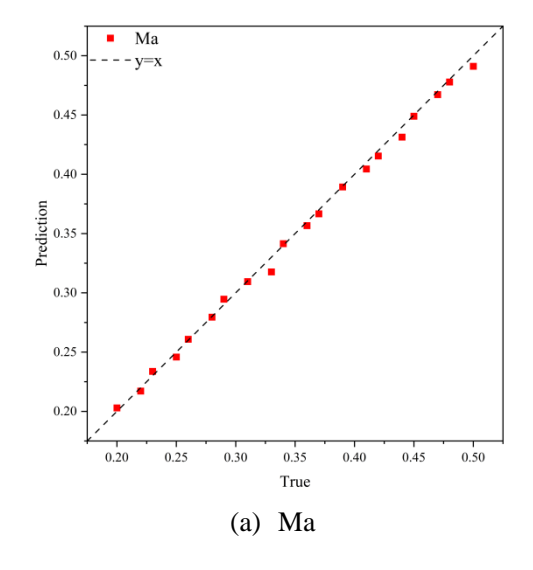
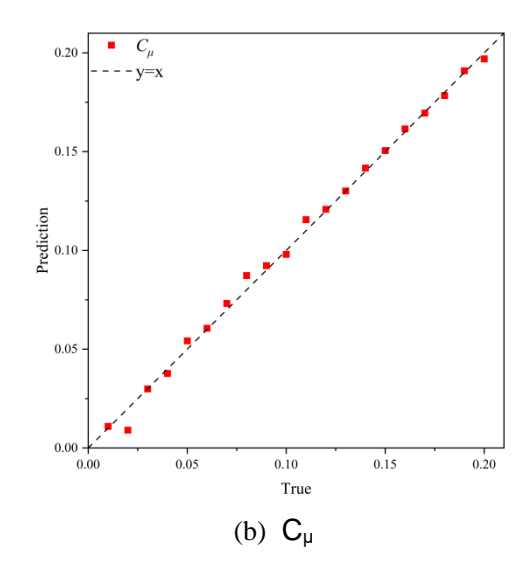
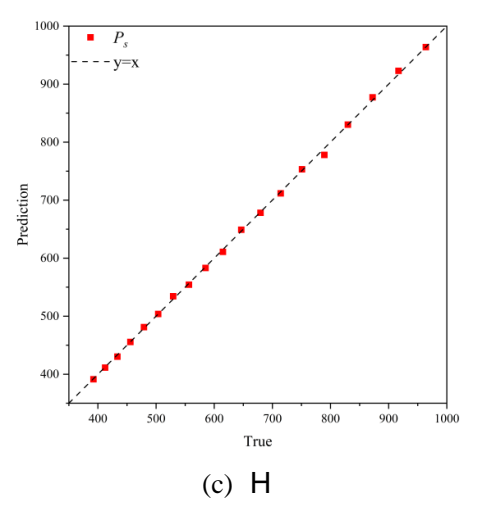


Figure 7 – The relative error box diagram of static pressure model.

After considered the stability and the accuracy of the model comprehensively, the Ma model with 40 neurons, the C_{μ} model with 40 neurons, the AoA model with 40 neurons and the P_s model with 30 neurons are selected as the flight state perception models built by this paper in the final. To assess their generalization ability, 20 groups of flight states and their corresponding pressure data are randomly generated. These data are input into each model to output Mach number, jet momentum coefficient, static pressure, and angle of attack, simulating real-world use. As shown in Figure 8, the test results show that the prediction value matches well with the true value, indicating that these models can predict the flight state parameters accurately.







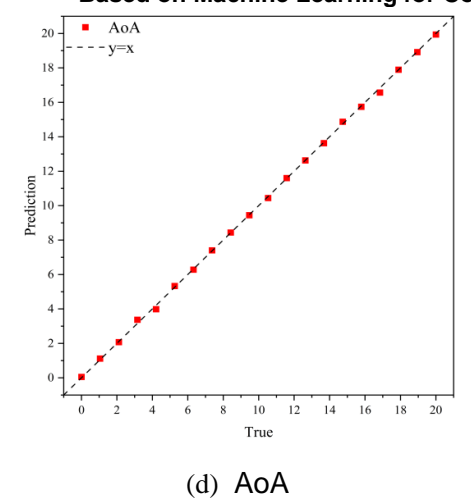


Figure 8 - Test results of four flight state perception models.

3. Fault diagnosis of flight state perception model

In practice, when the pressure sensor breaks down, the whole flight state perception system should have the ability to identify and eliminate the fault point, so as to ensure the input of the flight state perception models is correct and the system can accurately predict the flight state parameters. It has been proved in paper [15] that it is almost impossible to have more than one sensor fail during one flight. Therefore, this paper builds fault diagnosis classifiers only for the case where only one of the pressure sensors fails.

To make the fault diagnosis classifiers have the ability of identify specific fault point, this paper trains six classifiers corresponding to six pressure points relatively. For a pressure sensor point P_i (i=1,2,... 6), when establishing a fault diagnosis classifier, a relative error of larger than 10% should only be randomly added to the normal pressure value of the pressure point P_i in the data set used for training the model, while the pressure value of other pressure points should remain unchanged. If an error is added, the tag of the pressure group will be "1"; if no error is added, the tag should be "0". The data set contains 20,000 groups of pressure value of six pressure measurement points on the surface of the CFJ0012 airfoil listed in Table 1. Pressure value are generated by Kriging models constructed in section 2.2.

In this paper, the random forest classification algorithm is used to construct fault diagnosis classifiers. The initial step in employing the random forest classification algorithm for building fault diagnosis classifiers involves parameter adjustment. When tuning parameters, each parameter is considered in turn according to its importance for the model. Subsequently, a grid search is conducted within a small range of parameters. After tuning, the optimal parameter combination for each classifier is obtained, as shown in Table 2. Next, the dataset is split into training and test sets at a ratio of 7:3, and the parameters listed in Table 2 are used to train random forest classifiers, resulting in random forest models for each classifier.

Table 2 - The optimal parameter combination of each classifier.

Classifier number	1	2	3	4	5	6
N estimators	189	190	54	190	190	190
Max depth	29	24	26	24	24	29
Min samples split	4	4	9	4	4	4
Min samples leaf	3	3	6	3	3	3
Max features	0.1	0.1	0.1	0.1	0.1	0.1
criterion	gini	entropy	gini	entropy	entropy	entropy

In practice, which pressure point breaks down and weather the fault occurs are both random. Therefore, it is necessary to couple several fault diagnosis classifiers to test whether they can still diagnose faults and have the ability to diagnose the specific fault point when they work together. 100 groups of pressure $\{P_1, P_2, ..., P_6\}_{n=1,2,...,100}$ are used as test samples. On the basis of each group of pressures, a random pressure point is selected, and on the basis of its normal value, there is a 50% possibility of artificial fault addition to constitute the test data set. Combining six classifiers with default classification threshold for fault diagnosis, the test result is shown in Table 3. The fractional data in the table represents the ratio of the number of correctly identified faults to the total number of identified faults. It can be seen from the table that when all classifiers work together, the effect of fault diagnosis is not ideal.

Table 3 - Test results of the classifiers.

Pressure point ID	1	2	3	4	5	6
Number of faults	10	8	11	6	7	7
Result of fault diagnose	4/4	2/2	11/17	5/6	6/6	7/9

Therefore, to improve the fault diagnosis accuracy, indexes such as "Accuracy", "Precision" and "Recall" should be considered. The indexes mentioned above are calculated through confusion matrix shown in Table 4.

Table 4 - Confusion matrix.

Confusio	an matrix	Predicted value			
Confusion matrix		Negative	Positive		
Two volue	Negative	True negative (TN)	False positive (FP)		
True value —	Positive	False negative (FN)	True positive (TP)		

The most straightforward indicator to measure a classification model is "Accuracy," which represents the proportion of correctly classified samples in the total number of samples. "Accuracy" is calculated as $\frac{TP+TN}{TP+FP+TN+FN}$. "Precision" represents the ratio of the predicted positive samples that are actually positive, and its calculation formula is $\frac{TP}{TP+FP}$. "Recall" represents the ratio of positive cases predicted by the classifier to all actual positive cases. The formula for "Recall" is $\frac{TP}{TP+FN}$.

If malfunction happens, then the case is positive, and the tag of the case is set as "1". On the contrary, the case is negative with a tag as "0". In order to find the optimal threshold on the basis of the optimal classifier parameters and further optimize the classification effect of the model, the PR curves of each classifier are obtained, as shown in Figure 9. The horizontal coordinate of the PR curve is the "Recall", and the vertical coordinate is the "Precision". For a fault diagnosis task, the cost of missing judgment (that is, the fault is missed as no fault) is more serious than that of wrong judgment (that is, the fault is misjudged as no fault). Therefore, when selecting the threshold of each classifier, high recall value should be taken as the basis, and then take the high accuracy rate into account. The threshold corresponding to high recall rate and high precision rate of each classifier are shown in Table 5.

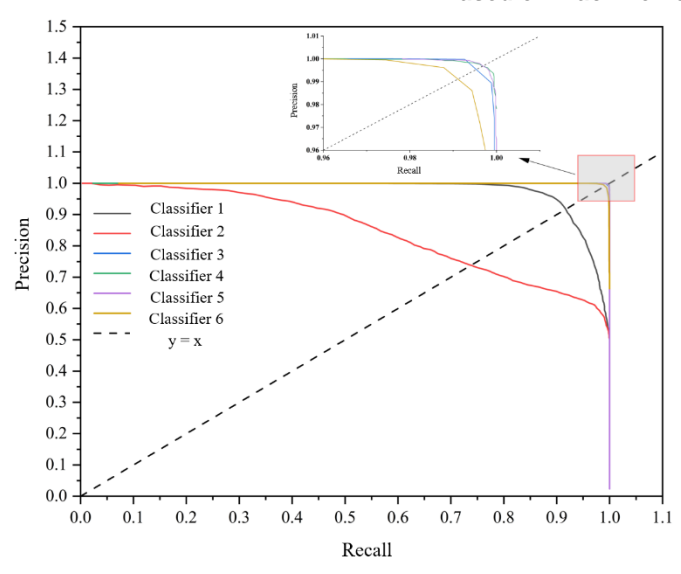


Figure 9 – PR curve of each classifier.

Table 5 – The threshold corresponding to high recall and high precision of each classifier.

				<u>U</u>		
Classifier ID	1	2	3	4	5	6
Threshold of high Recall	0.04	0.03	0.13	0.36	0.13	0.06
Threshold of high Accuracy	0.80	0.66	0.58	0.83	0.63	0.63

To test the fault diagnosis performance of each classifier, classifiers with different threshold are applied to carry out fault diagnosis, and the test result is shown in Table 6. The default threshold is 0.5, and the adjusted threshold is the threshold obtained after balancing high "Recall" and the high "Accuracy". It can be seen from Table 6 that under high "Recall" threshold, classifiers tend to identify malfunctions as many as possible, while the prediction accuracy is pretty low. Under high "Precision" threshold, the times of the classifier identifying faults is greatly reduced, however, the prediction accuracy is high. Under the adjusted threshold, the classifier 1, 3, 4 and 6 can recognize all malfunctions, and the classifier 2 and 5 can identify most of the malfunctions. That is to say, after threshold adjustment, the fault diagnosis ability of classifiers working together is greatly improved compared to the result shown in Table 3.

Table 6 - Test results of classifiers with different threshold.

I		results of Cic	199111612 MILLI	illierent tilles	noiu.	
Pressure point ID	1	2	3	4	5	6
Number of malfunctions	10	8	11	6	7	7
Default threshold	5/5	2/2	11/17	6/6	6/7	7/7
High "Recall" threshold	8/18	7/21	11/17	6/15	6/7	6/13
High "Accuracy" threshold	2/2	2/2	11/17	5/5	6/6	6/6
Threshold after adjustment	10/13	7/15	11/17	6/6	6/6	7/7

4. Fault-tolerance system of the flight state perception model

The malfunctions of the pressure measuring points can impact the accuracy of flight state perception models, leading to significant deviations in the prediction results. To prevent this phenomenon, this section integrates a fault diagnosis method with the flight state perception model to construct a fault-tolerance system specifically designed for the CFJ0012 airfoil's flight state perception models. The purpose is to enhance the robustness of the flight state perception model.

Figure 10 illustrates the construction process of the fault-tolerance system for the flight state perception model. Initially, the pressure value of six pressure measurement points are input into the fault diagnosis classifiers, which were constructed in Section 3, to detect the faults and identify the specific faulty point. If the fault is detected, the pressure values of the remaining five pressure measurement points are input into the flight state perception and fault-tolerance models, which output four flight state parameters. However, if a fault is not detected, the pressure values of all six pressure measuring points are utilized as inputs to the flight state perception model, which also outputs four flight state parameters. The fault-tolerance models here refer to the six flight state perception models with inputs of five pressure measurement points (excluding the fault point) constructed by deep neural network.

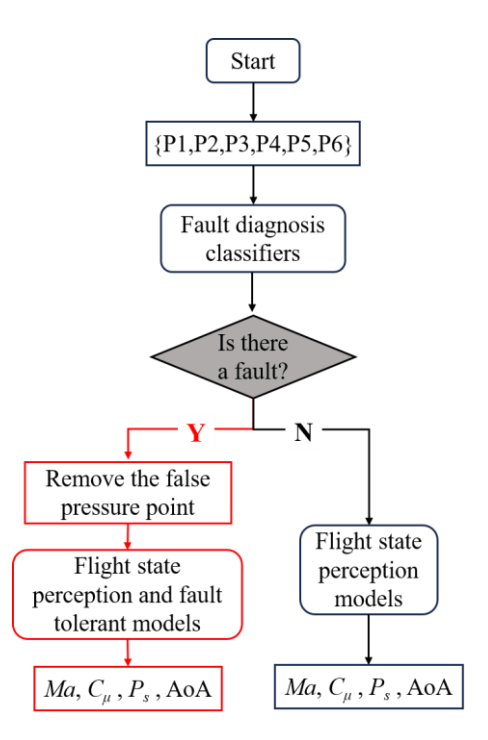


Figure 10 - Flow chart of fault tolerance system for flight state perception model.

The fault tolerance system for the flight state perception model, as shown in Figure 10, is coded using Python. To test the effectiveness of this system, 100 test samples which are same to what are used as test samples in section 3 are employed. The comparison between the predicted flight state parameters, both with and without fault diagnosis, and the true values is presented in Figure 11 (a)-(d). From the graphs, it is evident that after fault diagnosis, the predicted flight state parameters closely match the true values. However, without fault diagnosis, directly inputting the test dataset into the flight state perception models leads to significant deviations between the predicted flight state parameters and the true values. This indicates that the fault tolerance system constructed in this section significantly improves the robustness of the flight state perception model.

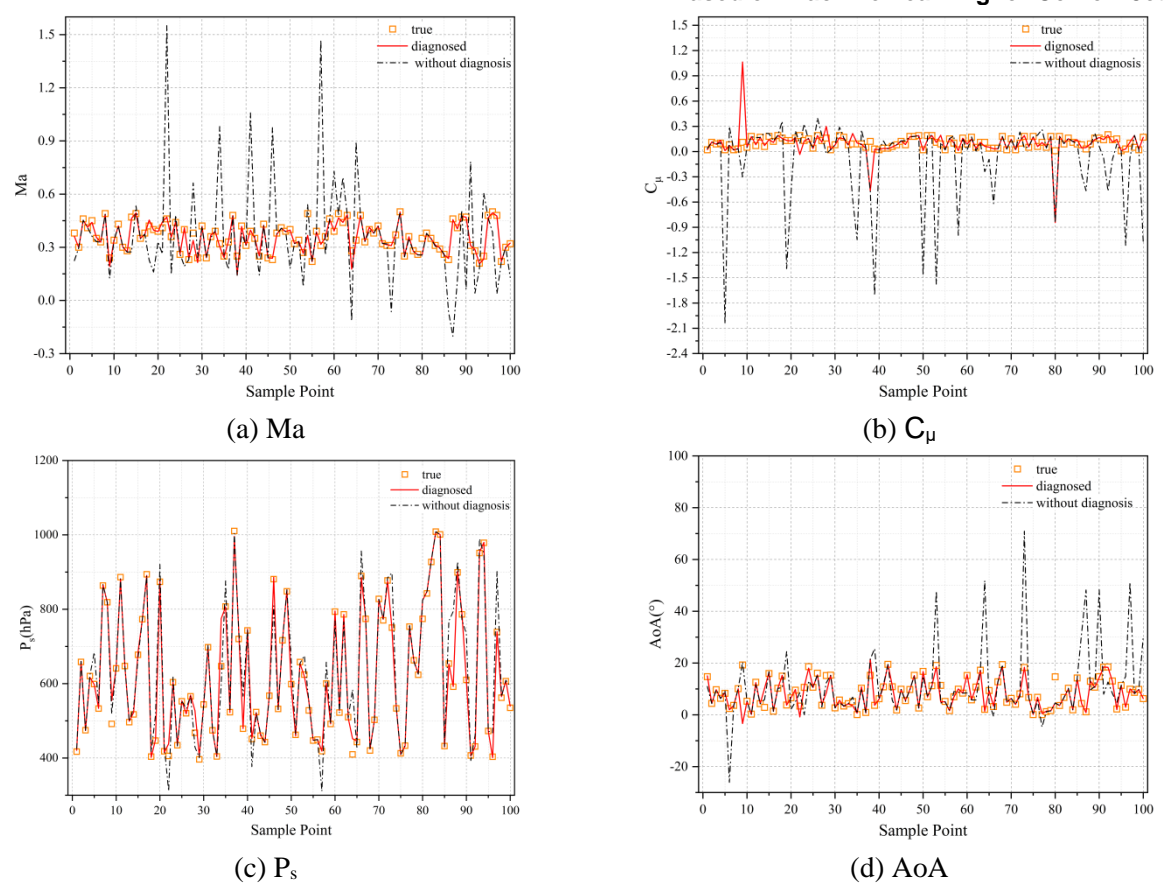


Figure 11 - Comparison of the prediction results by fault-diagnosed and undiagnosed flight state perception models.

5. Conclusion

This paper presents flight perception models based on deep neural networks, which are capable of extracting the Mach number, jet momentum coefficient, static pressure, and angles of attack of a CFJ airfoil from the pressure values measured at six points on the airfoil surface. To minimize prediction errors, deep neural networks with varying numbers of neurons are trained, and the best models are selected after error analysis. The static pressure model demonstrates the highest prediction precision, with a relative error of no more than 0.7%, while the jet momentum coefficient model exhibits lower accuracy, with a relative error of no more than 15%. These models enable real-time monitoring of the flight status of the CFJ airfoil, thereby facilitating the design of closed-loop control laws.

In order to enhance the robustness of the flight state perception models and ensure their accuracy in the event of a pressure sensor failure, the paper also introduces a fault diagnosis and fault tolerance method based on machine learning algorithms. This method significantly improves the robustness of the flight state perception models by effectively mitigating the impact of serious deviations between predicted and true values.

Given that the objective of this paper is to provide inputs for the closed-loop control system of the CFJ airfoil, future work will focus on integrating these models into the design of closed-loop control laws for the CFJ airfoil, enabling it to adjust its jet intensity in response to changes in flight state.

6. Contact Author Email Address

Zhao Yiran: 2021200017@mail.nwpu.edu.cn

7. Copyright Statement

The authors confirm that they, and/or their company or organization, hold copyright on all of the original material included in this paper. The authors also confirm that they have obtained permission, from the copyright holder

of any third party material included in this paper, to publish it as part of their paper. The authors confirm that they give permission, or have obtained permission from the copyright holder of this paper, for the publication and distribution of this paper as part of the ICAS proceedings or as individual off-prints from the proceedings.

References

- [1] Cary J P and Keener E R. Flight evaluation of the X-15 ball-nose flow-direction sensor as an air-data system. *NASA-TN-D-2923*, Washington, D. C., pp 1-19, 1965.
- [2] Brown E N, Friehe C A and Lenschow D H. The use of pressure fluctuations on the nose of an aircraft for measuring air motion. *Journal of Applied Meteorology and Climatology*, Vol. 22, No. 1, pp 171-180, 1983.
- [3] Larson T J, Whitmore S A and Ehernberger L J. Qualitative evaluation of a flush air data system at transonic speeds and high angles of attack. *NASA-TP-2716*, Washington, D. C., pp 1-61, 1987.
- [4] Larson T J, Moes T R and Siemers P M. Wind-tunnel investigation of a flush airdata system at Mach numbers from 0.7 to 1.4. *NASA-TM-101697*, Washington, D. C., pp 1-31, 1990.
- [5] Whitmore S A. Development of a pneumatic high-angle-of-attack flush airdata sensing system. *NASA-T-M-104241*, California, pp 1-24, 1991.
- [6] Whitmore S A and Moes T R. Measurement uncertainty and feasibility study of a flush airdata system for a hypersonic flight experiment. *Applied Aerodynamics Conference*, Colorado, pp 1-20, 1994.
- [7] Rohloff T J and Catton I. Development of a neural network flush airdata sensing system. Proceedings of the 1996 ASME International Mechanical Engineering Congress and Exposition, Atlanta, Vol. 242, IMECE1996-0952, pp 39-43, 1996.
- [8] Rediniotis O K and Vijayagopal R. Miniature multihole pressure probes and their neural-network-based calibration. *AIAA Journal*, Vol. 37, No 6, pp 666-674, 1999.
- [9] Samy I, Postlethwaite I and Gu D W. Neural-network-based flush air data sensing system demonstrated on a mini air vehicle. *Journal of Aircraft*, Vol. 47, No. 1, pp 18-31, 2010.
- [10]Ellsworth J C and Whitmore S A. Simulation of a flush air-data system for transatmospheric vehicles. *Journal of Spacecraft and Rockets*, Vol. 45, No. 4, pp 716-732, 2012.
- [11]Wu Y L, LI X D, Shan X W and Chen Y. Evaluation and improvement of five-hole pressure probe's performance at large AoA based on ANN. *AIAA AVIATION 2022 Forum*, Chicago, AIAA-2022-4152, pp 1-10, 2022.
- [12]Zha G C and Paxton C. A novel airfoil circulation augment flow control method using co-flow jet. 2nd AIAA Flow Control Conference, Portland, AIAA-2004-2208, pp 1-13, 2004.
- [13]Rohloff T J and Whitmore S A. Air data sensing from surface pressure measurements using a neural network method. *AIAA Journal*, Vol. 36, No 11, pp 2094-2101, 1998.
- [14]Zhao Y R, Xu H Y and Xie Z Y. Closed-loop flow control method based on deep reinforcement learning using a co-flow jet. *Journal of Applied Fluid Mechanics*, Vol. 17, No. 4, pp 816-827, 2024.
- [15]Zhang R, Du H, Wu Y, Qin X, and Zhang P. Fault detection and diagnosis for thrust drop of launch vehicles against disturbances. *Journal of Spacecraft and Rockets*, Vol. 60, No. 3, pp 924-941, 2023.